Sliding Mode Control for Space Debris Elimination

Hirohisa KOJIMA
Tokyo Metropolitan University, Hino, Tokyo, 191-0065, Japan

I. Introduction

Simple and reliable controllers are generally desired for spacecraft control, because it is very difficult to repair spacecraft on orbit. Classical control methods, such as PI, or PID, are simple and still quite often used for spacecraft control. Those linear control methods are, however, not adequate for conducting formation flight, which is a key technology to conduct feature space mission such as space telescope by multi-satellite, mitigation of space debris from orbit by flying around, approaching, and grasping the debris by means of a space robot. Because the motion required to the satellite conducting formation flying is nonlinear due to coupling between the attitude and position of the satellite relative to the other satellites. In addition, the malfunctioning target satellite is not always cooperative with the chaser, that is, motion of the target satellite may not be controlled by the chaser satellite, and is hard to predict because its inertia properties, which dominate the rotational motion, are not precisely known by the chaser in advance. These coupling and uncertainties or device fault situation may make the control problems more difficult. Thus it is desired to develop more suitable control methods for relative position/attitude control problem in space debris mitigation operation and extension of spacecraft lifespan. Sliding mode control can be such one of the promising control methods to meet this requirement, because it has desired properties such as simplicity of design, control of independent motion, invariance to process dynamics characteristics, and robustness to external perturbations. Those desired characteristics lead to wide variety of operational modes such as regulation, trajectory control, model following, and observation. Thanks to those good properties of sliding mode control, a great deal of applications of sliding mode control to spacecrafts has been studied up to date. The following are examples: formation flying, attitude control, space-robot manipulator control, and two-torque control.

However, by comparing the candidate debris elimination process or extension of spacecraft lifespan with the properties of the usual sliding model control method, it is found that the controllers do not still have sufficient properties for the requirements. The following are deficiencies of the usual sliding mode controllers in case of using them for debris mitigation, or extension of a spacecraft lifespan.

(1) Although it is assumed in the operation that cameras are used for inspecting the target, a function to prevent the violation of the chaser's line of sight (LOS) constraint is not explicitly formulated in the controller.
(2) Although the rotational motion behavior of the target depends on its moment inertia, and its uncertainties make the attitude-tracking problem more difficult, an adaptive law to estimate the moment inertia is not combined to the controller.
(3) Although it is difficult to repair the satellite on-board devices on orbit, a case of PWPF modulator fault is not considered for the two-control torque problem.

The research objective of this paper is to overcome these deficiencies of existing research by modifying the sliding-mode controllers. The following two topics are focused: fly-around motion, and an under-actuated control that may extend the lifespan of a satellite with malfunctioning RCS.

II. Fly-around Motion Control Based on Exact Linearization with Adaptive Law

Research Background

Several schemes have been proposed for attitude control problems[1-15]. For debris eliminating, fly-around motion must first be achieved because this motion is suitable for determining condition of a malfunctioning satellite. In order to achieve this motion, the development of an advanced control scheme for large-position and large-angle maneuvers is needed. Furthermore, if an on-board sensor on the chaser satellite, such as a camera, is the only means used to measure the relative position and attitude, tracking control based on the LOS angles is required. The LOS angles are nonlinear systems due to the dependence on the relative position and attitude between the target satellite and the chaser satellite. Therefore, the position and attitude of the chaser satellite relative to the target satellite are difficult to control by traditional linear schemes such as the linear quadratic regulator (LQR) method and are not able to be controlled independently if the tracking control is based on the LOS angles. The sliding-mode control technique is a nonlinear control method that has been applied in the position and attitude-tracking problem in [11]. The exact (or complete) linearization method [12] is another powerful method for controlling nonlinear systems. This method linearizes a nonlinear system by utilizing a nonlinear transformation of state variables and nonlinear feedback terms. Dwyer el al.[13] have proposed an exact nonlinear controller in which a reaction wheel is applied to the attitude control problem. Kida et al.[14] have studied a position and attitude regulation problem using an exact linearization method. However, their method was based on the Euler angle representation, and the singular problem of orientation representation was not avoided in the formulation. In [15], a method based on exact

linearization was proposed for the position and attitude control problem in which the listing parameter was used to represent the relative attitude. This parameter is not as common as quaternions because this parameter is not suitable for representing the relationship between the angular velocity and the derivative of the parameter. For this reason, some terms in the formulation are neglected for the exact linearization in [15]. Moreover, the inertia of the target satellite was assumed to be known in [15]. This assumption is not satisfied in reality, because determining exactly the inertia of a malfunctioning target satellite in advance is almost impossible.

In this chapter, an exact-linearization formulation is introduced, utilizing quaternions to represent the relative attitude of satellites. In the formation, control inputs are calculated from the relative position and attitude, line of sight(LOS) parameters, and the angular velocity of the chaser satellite, which can be measured on the chaser satellite. In other words, the control scheme does not require measurement of the absolute position of the chaser satellite in the inertia frame. LOS is defined based on the position of the target on a camera screen on the chaser satellite. This parameter can be controlled independently from the relative attitude, because the LOS angles depend on not only relative attitude, but also on relative position, and are decoupled from the relative attitude motion by controlling the relative position of the chaser satellite via the proposed nonlinear control scheme. The proposed control method is thus suitable for achieving fly-around motion, as well as multiple spacecraft formation flight, using an on-board sensor on the chaser satellite. Furthermore, an adaptive law is added to the present nonlinear controllers to estimate the inertia ratios of the target satellite. This law is effective for the case in which the target is a non-cooperative satellite. The effectiveness of the proposed exact-linearization method is demonstrated by numerical simulations.

Model Description

In this chapter, the satellite maneuvering near the target satellite is referred to as the chaser satellite. Figure 1 shows the system model treated in this study. When gravitational and orbital influences such as the Coriolis force are neglected, the equations of motion and attitude kinematics for the chaser satellite and the target satellite can be represented as follows:

$$m_c v_c + m_c \omega_c \times v_c = f_c \tag{1-1a}$$

$$I_c \omega_c + \omega_c \times I_c \omega_c = t_c \tag{1-1b}$$

$$\dot{q}_c = \frac{1}{2}\Omega(\omega_c) q_c \tag{1-1c}$$

$$m_t v_t + m_t \omega_t \times v_t = 0 \tag{1-2a}$$

$$I_t \omega_t + \omega_t \times I_t \omega_t = 0 \tag{1-2b}$$

$$\dot{q}_t = \frac{1}{2}\Omega(\omega_t) q_t \tag{1-2c}$$

where the subscripts c and t denote the chaser and target satellite, respectively, f_c and t_c are the control forces and torques, respectively, given to the chaser satellite, r, v, ω and q are the position, velocity, angular velocity and quaternions, respectively, of the satellites in their body-fixed frames, m and I are the mass and the inertia tensor, respectively, of the satellites and

$$\Omega(\omega) = \begin{bmatrix} -\omega^{\times} & \omega \\ -\omega^{T} & 0 \end{bmatrix} \tag{1-3}$$

The notation $x^{\times}, x = [x_1\ x_2\ x_3]^T$ denotes the following skew-symmetric matrix:

$$x^{\times} = \begin{bmatrix} 0 & -x_3 & x_2 \\ x_3 & 0 & -x_1 \\ -x_2 & x_1 & 0 \end{bmatrix} \tag{1-4}$$

The elements of the quaternions $q = [\tilde{q}^T q_4]^T = [q_1, q_2, q_3, q_4]^T$ are defined as follows:

$$q_1 = \lambda_1 \sin(\beta/2) \tag{1-5a}$$

$$q_2 = \lambda_2 \sin(\beta/2) \tag{1-5b}$$

$$q_3 = \lambda_3 \sin(\beta/2) \tag{1-5c}$$

$$q_4 = \cos(\beta/2) \tag{1-5d}$$

where $\lambda = [\lambda_1\ \lambda_2\ \lambda_3]^T$ is the direction cosine of the Euler unit vector and β is the rotation angle about the Euler vector. Any set of quaternions satisfies

$$\tilde{q}^T \tilde{q} + q_4^2 = 1 \tag{1-6}$$

In this study, differences in position, velocity, and angular velocity between the chaser and target are defined in the frame of the chaser satellites as follows:

$$r_e = r_c - C_t^c r_t \tag{1-7}$$

$$v_e = v_c - C_t^c v_t \tag{1-8}$$

$$\omega_e = \omega_c - C_t^c \omega_t \tag{1-9}$$

where C_t^c is the direct cosine matrix between the body frame of the chaser satellite and that of the target satellite. This matrix can be represented using the relative quaternions as follows:

$$C_t^c = (q_{e4}^2 - \tilde{q}_e^T \tilde{q}_e) U_{3\times 3} + 2\tilde{q}_e \tilde{q}_e^T - 2q_{e4}\tilde{q}_e^{\times} \tag{1-10}$$

where $U_{3\times 3}$ is the 3×3 unit matrix. The attitude error is defined as follows:

$$q_e = Q_1(q_t) q_c \tag{1-11}$$

where

$$Q_1(q)=\begin{bmatrix} q_4 U_{3\times3}-\tilde{q}^{\times} & -\tilde{q} \\ \tilde{q}^T & q_4 \end{bmatrix} \quad (1\text{-}12)$$

It is not difficult to show that the attitude error satisfies the following equation:

$$\tilde{q}_e^T\tilde{q}_e+q_{e4}^2=1 \quad (1\text{-}13)$$

Since Eq.(1-1c) or Eq.(1-2c) can be used to represent the kinematics of the attitude errors between the chaser satellite and the target satellite, the first derivative of quaternion errors is obtained as follows:

$$\dot{q}_e=\frac{1}{2}\Omega(\omega_e)q_e \quad (1\text{-}14)$$

Equations (1-13) and (1-10) indicate that when $\|\tilde{q}_e\|^2=0$, the direct cosine matrix C_t^c becomes the eigen matrix ($=U_{3\times3}$). From Eq.(1-14), the angular velocity error can be represented using the quaternion errors (q_e) as follows:

$$\omega_e=2\left[q_{e4}U_{3\times3}-\tilde{q}_e^{\times} \quad -\tilde{q}_e\right]\dot{q}_e \quad (1\text{-}15)$$

Thus, the attitude errors and angular velocity errors become zero when $\|\tilde{q}_e\|$ and $\|\tilde{\dot{q}}_e\|$ become zero. The objective of the following section is to obtain a nonlinear transformation and a feedback control which can convert the nonlinear system into an exact-linearized system. First, the definition of line of sight parameters will be explained. Second, the state vector will be defined, and the corresponding derivatives will be derived. Finally, an exact-linearization feedback controller based on the LOS parameters will be derived.

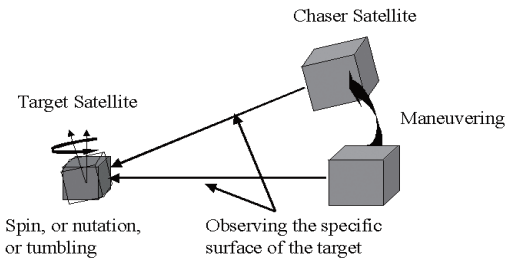

Fig.1 Schematic view of fly-around motion

Line of Sight Parameter

In this section, the definition of line of sight (LOS) parameters as applied in this chapter will be explained. The following assumptions are made: (1) the direction of the camera sight is coincident with the $-x$ direction of the body frame of the chaser satellite, (2) the relative distance of the target in the x direction and the velocity of the target on the camera screen can be sensed by the chaser.

Although the LOS angle is usually referred to as the relative angle between the sight direction of the camera on the chaser satellite and the direction from the chaser to the target, the LOS angle parameter is defined in this paper as follows:

$$L_{ang}=\begin{bmatrix} r_{ex} & d_y & d_z \end{bmatrix}^T=\begin{bmatrix} r_{ex} & s\dfrac{r_{ey}}{r_{ex}} & s\dfrac{r_{ez}}{r_{ex}} \end{bmatrix}^T \quad (1\text{-}16)$$

where s is the focus distance of the camera, and d_y and d_z are the y and z coordinates, respectively, indicating the position of the target on the camera screen, as shown in Fig.2. Note that s can be set as 1 without loss of generality.

The first and second derivatives of the position error can be represented using the position and velocity of the target on the camera screen as follows:

$$\dot{r}_{e_y}=\frac{d(d_y r_{e_x})}{dt}=\dot{d}_y r_{e_x}+d_y\dot{r}_{e_x} \quad (1\text{-}17a)$$

$$\dot{r}_{e_z}=\frac{d(d_z r_{e_x})}{dt}=\dot{d}_z r_{e_x}+d_z\dot{r}_{e_x} \quad (1\text{-}17b)$$

$$\ddot{r}_{e_y}=\ddot{d}_y r_{e_x}+d_y\ddot{r}_{e_x}+2\dot{d}_y\dot{r}_{e_x} \quad (1\text{-}18a)$$

$$\ddot{r}_{e_z}=\ddot{d}_z r_{e_x}+d_z\ddot{r}_{e_x}+2\dot{d}_z\dot{r}_{e_x} \quad (1\text{-}18b)$$

Solving the preceding equations with respect to $\ddot{d}_y$ and $\ddot{d}_z$, one has

$$\ddot{d}_y=-P_y\ddot{r}_{e_x}+P_x\ddot{r}_{e_y}-2P_x\dot{d}_y\dot{r}_{e_x} \quad (1\text{-}19a)$$

$$\ddot{d}_z=-P_z\ddot{r}_{e_x}+P_x\ddot{r}_{e_z}-2P_x\dot{d}_z\dot{r}_{e_x} \quad (1\text{-}19b)$$

where P_x, P_y and P_z are, respectively,

$$P_x=\frac{1}{r_{e_x}},\ P_y=\frac{r_{e_y}}{r_{e_x}^2}=\frac{1}{r_{ex}}d_y,\ P_z=\frac{r_{ez}}{r_{e_x}^2}=\frac{1}{r_{e_x}}d_z \quad (1\text{-}20)$$

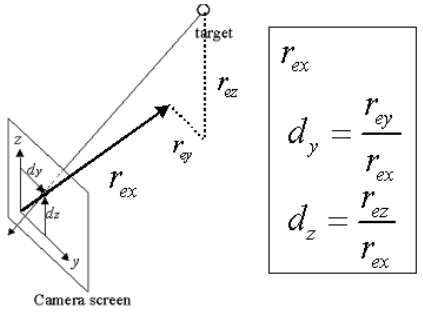

Fig.2 Definition of the line of sight

Relative Attitude

The derivative of quaternion error (Eq.(1-14)) can be rewritten as follows:

$$\dot{q}_e=\frac{1}{2}Q_2(q_e)\{\omega_c\}+\frac{1}{2}Q_3(q_e)\{\omega_t\} \quad (1\text{-}21)$$

where

$$Q_2(q_e)=\begin{bmatrix} q_{e4}U_{3\times3}+\tilde{q}_e^{\times} & \tilde{q}_e \\ -\tilde{q}_e^T & q_{e4} \end{bmatrix} \quad (1\text{-}22a)$$

$$Q_3(q_e)=\begin{bmatrix} -q_{e4}U_{3\times3}+\tilde{q}_e^{\times} & \tilde{q}_e \\ \tilde{q}_e^T & q_{e4} \end{bmatrix} \quad (1\text{-}22b)$$

$$\{\omega\}=[\omega^T\ 0]^T \quad (1\text{-}23)$$

The second derivative of q_e is obtained from Eq.(1-21) as follows:

$$\ddot{q}_e=\frac{1}{2}Q_2(\dot{q}_e)\{\omega_c\}+\frac{1}{2}Q_2(q_e)\{\dot{\omega}_c\}+\frac{1}{2}Q_3(\dot{q}_e)\{\omega_t\}+\frac{1}{2}Q_3(q_e)\{\dot{\omega}_t\} \quad (1\text{-}24)$$

The first three elements of the preceding derivative, $\ddot{\tilde{q}}_e$, can be rewritten as follows:

$$\ddot{\tilde{q}}_e=E_1(\dot{q}_e)\omega_c+E_1(q_e)\dot{\omega}_c-\{E_2(\dot{q}_e)\omega_t+E_2(q_e)\dot{\omega}_t\} \quad (1\text{-}25)$$

where

$$E_1=\frac{1}{2}(q_{e4}U_{3\times3}+\tilde{q}_e^{\times}) \quad (1\text{-}26a)$$

$$E_2=\frac{1}{2}(q_{e4}U_{3\times3}-\tilde{q}_e^{\times}) \quad (1\text{-}26b)$$

From Eqs.(1-1b) and (1-2b), one has

$$\dot{\omega}_c=I_c^{-1}(-\omega_c^{\times}I_c\omega_c+t_c) \quad (1\text{-}27)$$

$$\dot{\omega}_t=I_t^{-1}(-\omega_t^{\times}I_t\omega_t) \quad (1\text{-}28)$$

State Variables

It is assumed that the angular velocity of the chaser satellite can be measured on the chaser satellite using a device such as an inertia reference unit (IRU). Let parameter x consist of the angular velocity of the chaser satellite, relative position and attitude between the chaser and the target satellite, and the relative velocity and angular velocity as measured by the chaser satellite, as follows:

$$x=\begin{bmatrix}\omega_c^T & r_e^T & q_e^T & v_e^T & \omega_e^T\end{bmatrix}^T \quad (1\text{-}29)$$

and the error vector, which is used to represent the difference between the state of the chaser and that of the target satellite, be defined as follows:

$$e=\begin{bmatrix} r_e^T & \tilde{q}_e^T & v_e^T & \omega_e^T \end{bmatrix}^T \quad (1\text{-}30)$$

In addition, it is assumed that the position of the chaser relative to the target satellite in the x-direction of the body frame of the chaser, the LOS parameters, the relative attitude, and the derivatives of these variables can be measured on the chaser satellite. Under this assumption, the state vector $\hat{x}$ is defined as follows:

$$\hat{x}=\begin{bmatrix}\hat{x}_1^T & \hat{x}_2^T & \hat{x}_3^T & \hat{x}_4^T\end{bmatrix}^T=\begin{bmatrix} r_{e_x} & d_y & d_z & \tilde{q}_e^T & \dot{r}_{e_x} & \dot{d}_y & \dot{d}_z & \dot{\tilde{q}}_e^T \end{bmatrix}^T \quad (1\text{-}31)$$

Using Eqs.(1-29) and (1-30), Eq.(1-31) can be rewritten as follows:

$$\hat{x}=T(x)e \quad (1\text{-}32)$$

where

$$T(x)=\begin{bmatrix} R & O_{3\times3} & O_{3\times3} & O_{3\times3} \\ O_{3\times3} & U_{3\times3} & O_{3\times3} & O_{3\times3} \\ -P\omega_c^{\times} & O_{3\times3} & P & O_{3\times3} \\ O_{3\times3} & O_{3\times3} & O_{3\times3} & E_1(q_e) \end{bmatrix} \quad (1\text{-}33)$$

$$R=\begin{bmatrix} 1 & 0 & 0 \\ 0 & 1/r_{e_x} & 0 \\ 0 & 0 & 1/r_{e_x} \end{bmatrix} \quad (1\text{-}34)$$

$$P=\begin{bmatrix} 1 & 0 & 0 \\ -P_y & P_x & 0 \\ -P_z & 0 & P_x \end{bmatrix} \quad (1\text{-}35)$$

Nonlinear Control for Exact-Linearization

Let a nonlinear feedback control that includes forces and torques be as follows:

$$\begin{bmatrix} f_c \\ t_c \end{bmatrix}=\begin{bmatrix} \alpha_1(x) \\ \alpha_2(x) \end{bmatrix}+\begin{bmatrix} \beta_{11}(x) & \beta_{12}(x) \\ \beta_{21}(x) & \beta_{22}(x) \end{bmatrix}\begin{bmatrix} \hat{u}_1 \\ \hat{u}_2 \end{bmatrix} \quad (1\text{-}36)$$

where $\alpha_1(x)$ and $\alpha_2(x)$ are vectors $\in R^3$, $\beta_{11}(x)$, $\beta_{12}(x)$, $\beta_{21}(x)$ and $\beta_{22}(x)$ are matrices $\in R^{3\times3}$, and $\hat{u}_1$ and $\hat{u}_2$ are vectors $\in R^3$. From the preceding equation, one has

$$t_c=\alpha_2(x)+\begin{bmatrix}\beta_{21}(x) & \beta_{22}(x)\end{bmatrix}\begin{bmatrix}\hat{u}_1 \\ \hat{u}_2\end{bmatrix} \quad (1\text{-}37)$$

First, in order to obtain the nonlinear feedback torques, t_c, substituting Eqs.(1-27) and (1-37) into Eq.(1-1b), and letting the left-side of the equation become $\hat{u}_2$, the nonlinear functions for the exact linearization, $\alpha_2(x)$, $\beta_{21}(x)$ and $\beta_{22}(x)$, are obtained as follows:

$$\alpha_2(x)=\omega_t\times I_c\omega_t+I_cE_1^{-1}(q_e)\{E_2(\dot{q}_e)\omega_t+E_2(q_e)\dot{\omega}_t\}-I_cE_1^{-1}(q_e)E_1(\dot{q}_e)\omega_t \quad (1\text{-}38)$$

$$\beta_{21}(x)=O_{3\times3} \quad (1\text{-}39)$$

$$\beta_{22}(x)=I_cE_1^{-1}(q_e) \quad (1\text{-}40)$$

Next, in order to obtain the nonlinear feedback forces, f_c, one needs to consider the second derivative of r_{e_x}, d_y and d_z. The second derivatives of these variables can be represented by the second derivative of r_e, and r_e can be represented in the terms of r_{e_x}, d_y and d_z. Thus, in this section, the second-derivative of r_e is considered temporally

instead of the second-derivative of r_{e_x}, d_y and d_z, and the nonlinear feedback control force, which converts the position errors between the chaser and target satellites into an exact-linearized system. The first and second derivatives of r_e are represented as follows:

$$\dot{r}_e = v_e - \omega_c \times r_e \tag{1-41}$$

$$\ddot{r}_e = \frac{1}{m_c} f_c - 2\omega_c \times \dot{r}_e - \omega_c \times (\omega_c \times r_e) - \dot{\omega}_c \times r_e \tag{1-42}$$

where Eqs.(1-1a), (1-2a), (1-7) and the relation $\dot{C}_i^T = C_i^T \omega^{\times}$ ($i = c$ or t) are used.

Substituting Eqs.(1-27), (1-37), (1-38), (1-39) and (1-40) into Eq.(1-42), one has

$$\begin{aligned}\ddot{r}_e = {} & \frac{1}{m_c} f_c - 2\omega_c \times \dot{r}_e - \omega_c \times (\omega_c \times r_e) \\ & - E_1^{-1}(q_e)\left\{E_2(\dot{q}_e)\omega_t + E_2(q_e)\dot{\omega}_t\right\} \times r_e \\ & + E_1^{-1}(q_e)E_1(\dot{q}_e)\omega_c \times r_e \; - E_1^{-1}(q_e)\hat{u}_2 \times r_e\end{aligned} \tag{1-43}$$

From Eq.(1-36), the nonlinear feedback control force is represented as:

$$f_c = \alpha_1(x) + \begin{bmatrix}\beta_{11}(x) & \beta_{12}(x)\end{bmatrix}\begin{bmatrix}\hat{u}_1 \\ \hat{u}_2\end{bmatrix} \tag{1-44}$$

Substituting this control force into Eq.(1-43) and comparing both sides of equation in order to convert the relative position system into an exact-linearized system, the nonlinear functions $\alpha_1(x)$, $\beta_{11}(x)$ and $\beta_{12}(x)$ are obtained as follows:

$$\begin{aligned}\alpha_1(x) = {} & 2m_c\omega_c \times \dot{r}_e + m_c\omega_c \times (\omega_c \times r_e) \\ & + m_c E_1^{-1}(q_e)\left\{E_2(\dot{q}_e)\omega_t + E_2(q_e)\dot{\omega}_t\right\} \times r_e \\ & - m_c E_1^{-1}(q_e)E_1(\dot{q}_e)\omega_c \times r_e\end{aligned} \tag{1-45}$$

$$\beta_{11}(x) = m_c U_{3\times 3} \tag{1-46}$$

$$\beta_{12}(x) = -m_c r_e^{\times} E_1^{-1}(q_e) \tag{1-47}$$

Note that the preceding feedback control forces are used to convert the relative position system, rather than the LOS parameters, into an exact-linearized system. Therefore, an additional nonlinear feedback term and a transformation matrix are still necessary in order to exactly linearize the LOS parameter. In order to obtain the required term and matrix, let the position control force be considered by adding a nonlinear term α_1 and matrix D as follows:

$$f_c = \alpha_1(x) + \alpha_1(x) + \begin{bmatrix}\beta_{11}(x)D & \beta_{12}(x)\end{bmatrix}\begin{bmatrix}\hat{u}_1 \\ \hat{u}_2\end{bmatrix} \tag{1-48}$$

Substituting Eqs.(1-45), (1-46), (1-47) and (1-48) into Eq.(1-43), and taking Eqs.(1-19a) and (1-19b) into consideration, the additional nonlinear term α_1 and matrix D can be obtained, respectively, as follows:

$$\alpha_1(x) = \begin{bmatrix}0 \\ 2m_c \dot{r}_{e_x} \dot{d}_y \\ 2m_c \dot{r}_{e_x} \dot{d}_z\end{bmatrix} \tag{1-49}$$

$$D = P^{-1} \tag{1-50}$$

where P is a matrix defined in Eq.(1-35), and is invertiable if r_{e_x} is not zero, that is, if the difference between the chaser and target satellites in the x direction of the chaser body frame is not zero.

Consequently, an exact-linearized system and the nonlinear feedback control inputs for exactly linearizing the system, that consist of the LOS parameters, the relative attitude and their derivatives, can be represented as follows:

$$\dot{\hat{x}} = \hat{A}\hat{x} + \hat{B}\hat{u} \tag{1-51}$$

where

$$\hat{A} = \begin{bmatrix}O_{3\times 3} & O_{3\times 3} & U_{3\times 3} & O_{3\times 3} \\ O_{3\times 3} & O_{3\times 3} & O_{3\times 3} & U_{3\times 3} \\ O_{3\times 3} & O_{3\times 3} & O_{3\times 3} & O_{3\times 3} \\ O_{3\times 3} & O_{3\times 3} & O_{3\times 3} & O_{3\times 3}\end{bmatrix} \tag{1-52}$$

$$\hat{B} = \begin{bmatrix}O_{3\times 3} & O_{3\times 3} \\ O_{3\times 3} & O_{3\times 3} \\ U_{3\times 3} & O_{3\times 3} \\ O_{3\times 3} & U_{3\times 3}\end{bmatrix} \tag{1-53}$$

$$\begin{aligned}\alpha(x) = {} & \begin{bmatrix}\alpha_1(x) \\ O_{3\times 3}\end{bmatrix} + \begin{bmatrix}2m_c\omega_c \times \dot{r}_e + m_c\omega_c \times (\omega_c \times r_e) \\ \omega_c \times I_c\omega_c\end{bmatrix} \\ & + \begin{bmatrix}m_c E_1^{-1}(q_e)E_2(\dot{q}_e)\omega_t \times r_e \\ I_c E_1^{-1}(q_e)E_2(\dot{q}_e)\omega_t\end{bmatrix} + \begin{bmatrix}m_c E_1^{-1}(q_e)E_2(q_e)\dot{\omega}_t \times r_e \\ I_c E_1^{-1}(q_e)E_2(q_e)\dot{\omega}_t\end{bmatrix} \\ & - \begin{bmatrix}m_c E_1^{-1}(q_e)E_1(\dot{q}_e)\omega_c \times r_e \\ I_c E_1^{-1}(q_e)E_1(\dot{q}_e)\omega_c\end{bmatrix}\end{aligned} \tag{1-54}$$

$$\beta(x) = \begin{bmatrix}m_c D & -m_c r_e^{\times} E_1^{-1}(q_e) \\ O_{3\times 3} & I_c E_1^{-1}(q_e)\end{bmatrix} \tag{1-55}$$

From Eq.(1-54), it is found that the nonlinear function $\alpha(x)$ includes the derivative of the angular velocity of the target satellite. This derivative can be estimated using Eq.(1-2b) if the inertia of the target is known and the angular velocity of the target can be sensed. The case in which the inertia of the target is known is almost never satisfied in reality, because the target satellite is assumed to be a malfunctioning, non-cooperative satellite. In order to overcome the problem of the

preceding formulation, an adaptive law to estimate the inertia of the target will be described for a simple case in the next section.

After linearizing the system, any type of control method, such as LQR, can be employed for the exact-linearized system. However, the preceding linearizing formulation requires that matrices E_1 and P are not singular, which occurs when either q_{e4} or r_{e_x} is zero. Applying the LQR method to the preceding exact-linearized system cannot guarantee these requirements. The former singular case can be easily avoided by employing techniques, such as perturbation of the quaternions with small values or skipping control for a short period near the singularity. In the next section, the controller for avoiding both singular cases will be derived from a Lyapunov function that includes a repulsive potential for avoiding both singularities. The attitude part in the controller is basically equivalent to that in [15].

Design of Adaptive Law

In this section, an adaptive law for estimating the inertia ratios of the target satellite is designed under the assumption that the principal axis of the target satellite is coincident with its body axis, and the inertia tensor of the chaser is known exactly. This assumption is at least necessary. This is because the inertia ratios are dominant parameters for the rotational motion of a rigid body, and it is impossible to determine the orientation difference between the body frame and principal axis frame from only the angular velocities. The objective of the law is to improve the performance of the preceding exact-linearization controller. Attitude tracking error, and the velocity and angular velocity of the satellite are used to update the inertia parameters in this study. In order to quantify the parametric mismatch, the parameter estimation error is defined as follows:

$$\tilde{k} = k - \hat{k} \tag{1-56}$$

where k is constant, unknown vector of the inertia parameters and is defined as follows:

$$k = \begin{bmatrix} k_x & k_y & k_z \end{bmatrix}^T = \begin{bmatrix} (I_{t22} - I_{t33})/I_{t11} \\ (I_{t33} - I_{t11})/I_{t22} \\ (I_{t11} - I_{t22})/I_{t33} \end{bmatrix} \tag{1-57}$$

Let η and σ be defined, respectively, as:

$$\eta = a\hat{x}_1 + \hat{x}_3 \tag{1-58}$$

$$\sigma = b\hat{x}_2 + \hat{x}_4 \tag{1-59}$$

where a and b are constant, positive, definite, diagonal matrices or are simply constant scalars, $\hat{x}_2$, $\hat{x}_3$ and $\hat{x}_4$ are defined in Eq.(1-32), and $\hat{x}_1$ is defined as:

$$\hat{x}_1 = \begin{bmatrix} r_{e_x} - r_c & d_y & d_z \end{bmatrix}^T \tag{1-60}$$

A candidate Lyapunov function is selected as:

$$V = \frac{1}{2}\eta^T\eta + \frac{1}{2}\sigma^T\sigma + \frac{1}{2}i\left(1 - r_c/r_{e_x}\right)^2 + \frac{1}{2}j\hat{x}_2^T\hat{x}_2/(1 - \hat{x}_2^T\hat{x}_2) + \frac{1}{2}\tilde{k}^T G^{-1}\tilde{k} \tag{1-61}$$

where G is a constant positive definite diagonal matrix. Taking the time derivative of the preceding equation, one has

$$\dot{V} = \dot{\eta}^T\eta + \dot{\sigma}^T\sigma + ir_c\dot{r}_{e_x}(1 - r_c/r_{e_x})/r_{e_x}^2 + j\hat{x}_2^T\dot{\hat{x}}_2/(1 - \hat{x}_2^T\hat{x}_2) + \dot{\tilde{k}}^T G^{-1}\tilde{k} \tag{1-62}$$

Control inputs $\hat{u}_1$ and $\hat{u}_2$ are designed as follows:

$$\hat{u}_1 = -a\hat{x}_3 - c\eta + \hat{u}_1 \tag{1-63}$$

$$\hat{u}_2 = -b\hat{x}_4 - d\sigma + \hat{u}_2 \tag{1-64}$$

where $\hat{u}_1$ and $\hat{u}_2$ are, respectively,

$$\hat{u}_1 = \begin{bmatrix} -ir_c(1 - r_c/r_{e_x})/r_{e_x}^2 & 0 & 0 \end{bmatrix}^T \tag{1-65}$$

$$\hat{u}_2 = -j\hat{x}_2/(1 - \hat{x}_2^T\hat{x}_2)^2 \tag{1-66}$$

Substituting Eqs.(1-58)-(1-60), and (1-63)-(1-66) into Eq.(1-62), and taking the parameter mismatches (Eq.(1-56)) into account, the time derivative of the candidate Lyapunov function can be rewritten as follows:

$$\dot{V} = -air_c(r_{e_x} - r_c)^2/r_{e_x}^3 - bj\hat{x}_2^T\hat{x}_2/(1 - \hat{x}_2^T\hat{x}_2)^2 - c\eta^T\eta - d\sigma^T\sigma + \tilde{k}^T(Y_2^T\eta + Y_3^T\sigma + G^{-1}\dot{\tilde{k}}) \tag{1-67}$$

where

$$Y_2 = r_e^{\times} NE_2W \tag{1-68}$$

$$Y_3 = -E_2W \tag{1-69}$$

$$W = diag(\omega_{t2}\omega_{t3}, \omega_{t3}\omega_{t1}, \omega_{t1}\omega_{t2}) \tag{1-70}$$

If an adaptive law to estimate the inertia ratios of the target is designed as:

$$\dot{\tilde{k}} = -G(Y_2^T\eta + Y_3^T\sigma) \tag{1-71}$$

the time derivative of the candidate Lyapunov function (Eq.(1-67)) becomes

$$\dot{V} = -air_c(r_{e_x} - r_c)^2/r_{e_x}^3 - bj\hat{x}_2^T\hat{x}_2/(1 - \hat{x}_2^T\hat{x}_2)^2 - c\eta^T\eta - d\sigma^T\sigma \tag{1-72}$$

If the following conditions are satisfied at the initial time

$$r_{e_x}(0) > 0 \text{ and } \hat{x}_2(0)^T\hat{x}_2(0)(= \tilde{q}_2^T(0)\tilde{q}_e(0)) \neq 0 \tag{1-73}$$

From Eqs.(1-61), (1-67) and (1-73), it is easily shown that

$$0 \le V(t) \le V(0) < \infty \tag{1-74}$$

Thus, it is clear that $r_{e_x}(t) \neq 0$ and $\| q_e(t) \|_2 \neq 1$ for all time. Therefore, $N_1(\hat{x}_2)$ is always invertible, and r_{e_x} is always positive. This means that if the target can be seen on the on-board camera installed on the chaser satellite at the initial time, the target never escapes the camera screen as long as the control inputs (Eqs.(1-63)-(1-66)) and the adaptive law (Eq.(1-71)) are employed. In addition, it is obvious from Eq.(1-72) that r_{e_x} converges to r_c and d_y, d_z, $\dot{d}_y$, $\dot{d}_z$, $\dot{r}_{e_x}$, q_e and $\dot{q}_e$ asymptotically become zero as

time increases, that is, the chaser satellite can fly around the target satellite, tracking the attitude motion of the target correctly and maintaining the specified distance r_c from the target.

The estimated inertia ratios of the target satellite, $\hat{k} = [\hat{k}_x \ \hat{k}_y \ \hat{k}_z]^T$ are obtained by integrating the following equation based on the adaptive law (Eq. (1-71)):

$$\hat{k}(t) = \hat{k}(0) - \int_0^t \dot{\hat{k}} dt \qquad (1\text{-}75)$$

where $\hat{k}(0)$ is the estimated inertia ratios for the target satellite at the initial time.

Numerical Simulation

A. Simulation Parameters

Euler rotational motions are classified into four types according to the inertia ratio and angular velocities assuming no internal or external forces or torques on the rigid body: (1) non-symmetric rotational motion, (2) non-periodic rotational motion, (3) symmetric axis rotational motion, and (4) single-axis rotational motion. In this study, only a symmetric axis rotational motion is examined as the target attitude motion.

The validity of the proposed adaptive position and attitude tracking controller based on the exact linearization is verified numerically, compared with the position and attitude tracking controller without the adaptive law, where the chaser satellite is controlled to synchronize its attitude with that of the target satellite and to maintain its relative position to the target at some constant distance so as to avoid collisions with the target. The parameters of the numerical simulations are listed in Table 1.

The following numerical simulations are conducted.

- Case (a) The adaptive law to estimate the inertia ratios of the target satellite is not employed, even though the model parameter for the inertia ratios of the target satellite includes some errors.
- Case (b) The adaptive law to estimate the inertia ratios of the target satellite is employed.

The position of the target is assumed to be on the origin in the inertia frame for all cases. The angular velocities of the target about each axis are chosen as 0.1 rad/s at the initial time.

The performance of the adaptive law is assessed by setting the initial estimated inertia ratios of the target at the same erroneous value for Cases (a) and (b). As mentioned previously, the proposed controller is an adaptive sliding-mode controller including repulsive control inputs to avoid singularities. These repulsive control inputs could have an undesirable influence on the adaptive law used to estimate the parameters. Thus, in the present study, parameters i and j are set small (i.e., 0.001) so as to avoid to the greatest extent possible the effect of the repulsive control inputs on the adaptive law.

B. Simulation Results

The time response of the inertia ratios for the target as estimated by the adaptive law is shown in Fig. 3. The results for Cases (a) and (b) are shown in Figs.4 and 5, respectively. Each figure shows the time responses of LOS errors, quaternion error, control input force and control input torque for the chaser satellite. LOS errors are completely eliminated, but the attitude errors are not completely eliminated for Case (a) even after a long time (i.e. 500 s). This is because the controller for Case (a) does not include the adaptive law, and some errors are contained in the model of the target satellite. On the other hand, although the attitude errors for Case (b) change dramatically at the beginning of a tracking maneuver, the errors are completely eliminated after approximately 100 s, as shown in Fig.5. The correct values of the inertia ratios for the target are $k_x = -0.5$, $k_y = 0.5$, and $k_z = 0$.

The estimated inertia ratios converge to the correct values after approximately 150 s. From a comparison of Fig.4 with Fig.5, and taking the convergence of the estimated inertia ratios for the target satellite into account, the inclusion of the adaptive law improves the tracking performance of the exact-linearization controller effectively.

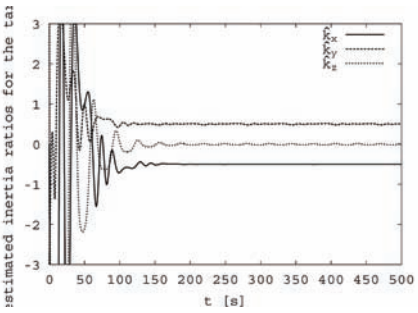

Fig.3 Time response of the estimated inertia ratios of the target satellite.

Table 1. Parameters for numerical simulations.

inertia	**target**	$I_{t11}=10 \quad I_{t22}=10 \quad I_{t33}=15\ \mathrm{kgm}^2$
	chaser	$I_c=\begin{bmatrix}300 & -30 & -50\\ -30 & 400 & -40\\ -50 & -40 & 300\end{bmatrix}\mathrm{kgm}^2 \qquad m_c=500\ \mathrm{kg}$
Initial state	**target**	$r_t=\begin{bmatrix}0 & 0 & 0\end{bmatrix}^T\ \mathrm{m} \quad q_t=\begin{bmatrix}0 & 0 & 0 & 1\end{bmatrix}^T$ $v_t=\begin{bmatrix}0 & 0 & 0\end{bmatrix}^T\ \mathrm{m/s} \quad \omega_t=\begin{bmatrix}0.1 & 0.1 & 0.1\end{bmatrix}^T\ \mathrm{rad/s}$
	chaser	$r_c=\begin{bmatrix}10 & 0 & 0\end{bmatrix}^T\ \mathrm{m} \quad \omega_c=\begin{bmatrix}0 & 0 & 0\end{bmatrix}^T\ \mathrm{rad/s}$ $v_c=\begin{bmatrix}0 & 0 & 0\end{bmatrix}^T\ \mathrm{m/s} \quad q_c=\begin{bmatrix}0 & 0 & \sqrt{2}/2 & \sqrt{2}/2\end{bmatrix}^T$
gains		$a=b=c=d=0.1,\ \ i=j=0.001\ \ G=4\times10^3 U_{3\times3}$

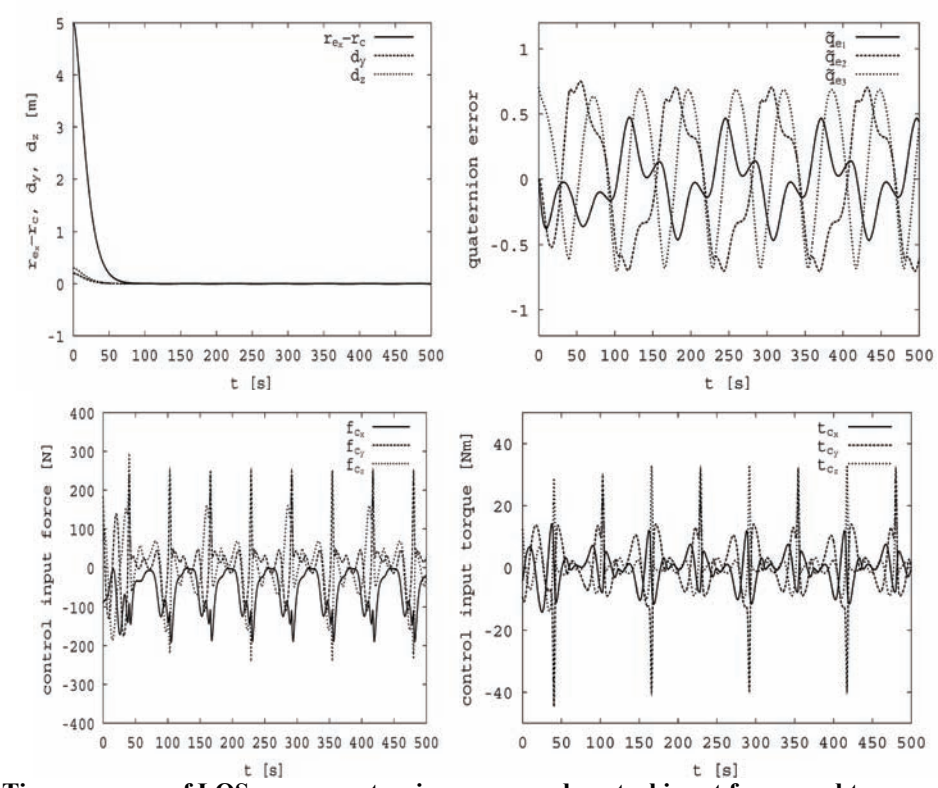

Fig.4 Time response of LOS error, quaternion error, and control input forces and torques for case (a).

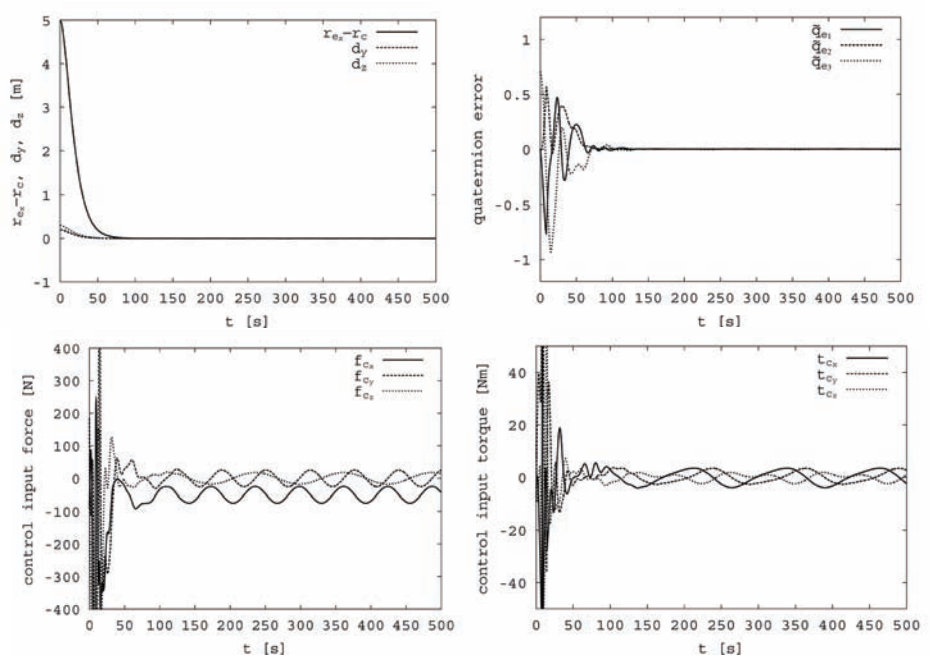

Fig.5 Time response of LOS error, quaternion error, and control input forces and torques for case (b).

III. Stabilization of Angular Velocity of Asymmetrical Rigid Body Using Two Constant Torques

Research Background

The problem of stabilization of angular velocity using less than three control torques has been investigated by several authors[16-26]. The present system can be stabilized by nonlinear control schemes, which may be categorized into three types: time-varying control schemes, discontinuous control schemes, and time-invariant control schemes. In those studies, it is assumed that an arbitrary magnitude of the torques can be fed to a satellite to attenuate its rotational motion using gas jet thrusters employing the Pulse Width Pulse Frequency (PWPF) Modulator. If thrusters provide two control torques without the use of PWPF, then the magnitude of the torque does not linearly respond to the input magnitude, and, indeed, is constant. No previous studies have considered this special case. If a control scheme could be derived for this case, then the resulting control method can facilitate a reduction in the use of PWPF modulation from satellites, or can form a backup system in the event of malfunction of the PWPF modulators, subject to the two-control-torque problem.

In this chapter, provided that the model uncertainties and external disturbances are neglected, a constant control torque method to attenuate the rotational motion of an asymmetric rigid body is proposed. The proposed control method is classed as a discontinuous and open loop control method. Because the magnitude of the control torque is constant, that is, it can only be applied On-Off, and the control timing is pre-determined. In this chapter, the set of angular velocities of an asymmetrical rigid body achievable by employing a single constant control torque is defined as “constant-torque-manifold” or simply referred to as the manifold. In the case when only a single constant control torque is used, this manifold can be analytically obtained by integrating the equations of motion backwards in time from the angular velocities that are accessible to the origin by employing a single constant control torque, where the set of angular velocities that can access the origin by a single constant control torque is hereafter referred to as a transient goal. A trajectory resulting from the proposed control method consists of three steps: If the polhode starting from initial angular velocities has intersection points with the manifolds, then the rotational motion does not need to be either boosted or damped. On the other hand, if the polhode starting from the initial angular velocities has no intersection points with the manifold, the rotational motion must be boosted around the maximum or minimum principal moment of inertia and damped around the middle principal moment of inertia to ensure that the trajectory has at least one point intersecting the manifolds. The first step is thus given by the trajectory of the angular velocities to an intersection point with the manifold, without the control torques, or boosted/damped by the control torques if necessary. The second step is a trajectory sliding on the manifold, by means of a single constant torque, until the transient goal is reached. The final step is a trajectory from the transient goal to the origin. The control timings, durations and the sign of control torques can then be

determined by calculating the intersection points between the manifold and polhode or the boosted/damped trajectory, between the trajectory sliding on the manifold and the transient goal, and between the single spin motion and the origin. A schematic representation of these trajectories is shown in Fig. 6. The idea of the constant-torque-manifold for stabilization of the rotational motion of an asymmetric rigid body is inspired by [27], which describes a method to obtain a trajectory of the angular velocities of an asymmetric rigid body when a single constant torque is employed along either the maximum, minimum, or middle principal moment of inertia axis. Contrary to the robust feedback schemes[24-26], a demerit of the proposed method is that it is not robust to the modeling errors, and external disturbances. On the other hand, a merit of the proposed method is that it can easily estimate the convergence time. This is because the manifolds are obtained analytically and the dynamic control problem is converted into a kinematics problem of the calculation of intersection points between the manifolds and polhode or boosted/damped trajectory, and this converted problem can be solved by the bi-section method. Results of a numerical simulation of the present method applied to a test problem are given later in this chapter to show that the complete attenuation can be achieved by using the proposed manifold, provided that external disturbances and modeling uncertainties are absent, and the intersection point between the manifolds and polhode or boosted/damped trajectories is completely obtained.

Problem Statement and Equations of Motion

Throughout this chapter, it is assumed that the principal axes of a satellite are coincident with its body frame coordinates. Because in this chapter, only the case of an asymmetrical rigid body, principal moments of inertia satisfy $j_1 \neq j_2 \neq j_3$ is treated. Without loss of generality, it is assumed that $j_1 > j_2 > j_3$. Referring to [27], the equation of motion can be rewritten in the form

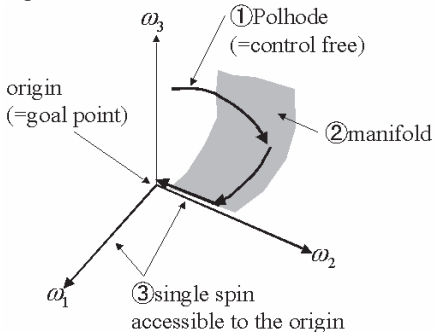

Fig. 6 Schematic view of the trajectory resulting from the constant control torque method.

$$\begin{bmatrix} x_1' \\ x_2' \\ x_3' \end{bmatrix} = \begin{bmatrix} x_2 x_3 \\ -x_3 x_1 \\ x_1 x_2 \end{bmatrix} + \begin{bmatrix} \mu_1 \\ \mu_2 \\ \mu_3 \end{bmatrix} \qquad (2\text{-}1)$$

where ()' denotes the derivative operator $d()/d\tau$ where τ is the scaled time, (x_1, x_2, x_3) is the scaled angular velocity vector and (μ_1, μ_2, μ_3) is the scaled constant torque vector. The detail of the variable changes is described in [27]. In this chapter, the derivation of a control method using less than three constant control torques that can attenuate the rotational motion of an asymmetric rigid body is considered.

Constant Control Torque Method

A. Transient Goals and Constant Torque Patterns

If the angular velocities along the uncontrolled axis and one of the remaining controlled axes are both zero, then the system is both controllable and accessible to the origin. This situation, which is a single spin motion around the one of the controllable axes, can be therefore treated as a transient goal. In this paper, the control torques are assumed to be generated by gas jet thrusters without using PWPF modulators. In this case, the torque takes a plus or minus sign, or can be zero in magnitude (i.e. switched off), and the total number of combinations of the signs of the thrusters is nine. Although all the above sets of signs of the control torques can be used to generate manifolds, the analytical manifolds can be obtained only for the case when a single constant control torque is not along one of the principal axes corresponding to the single spin motion. Therefore in this chapter, only this case will be considered.

Because there exist three possibilities for the uncontrolled axis; the maximum, middle, or minimum principal moment of inertia, and there are two cases for the single spin motion around the controllable axis, there thus exist six cases for generating the manifolds, as listed in Table 2.

B. Manifolds

The manifolds can be obtained by integrating the equations of motion backward in time from transient goals with the employment of a single constant control torque. With reference to [27], and taking the angular velocities of the transient goals into account, the manifold for each case in Table 2 can then be analytically obtained as follows:

(I)
$$x_1^2 = 2\mu_1\theta - A^2 \sin^2\theta \qquad (2\text{-}2a)$$
$$x_2 = -A\sin\theta \qquad (2\text{-}2b)$$
$$x_3 = A\cos\theta \qquad (2\text{-}2c)$$

Table 2. Transient Goals.

maximum	middle	minimum	transient goal*
(I) constant torque	uncontrollable	controllable	$x_1(0)=0, x_2(0)=0, x_3(0)\neq 0$
(II) constant torque	controllable	uncontrollable	$x_1(0)=0, x_2(0)\neq 0, x_3(0)=0$
(III) uncontrollable	constant torque	controllable	$x_1(0)=0, x_2(0)=0, x_3(0)\neq 0$
(IV) controllable	constant torque	uncontrollable	$x_1(0)\neq 0, x_2(0)=0, x_3(0)=0$
(V) controllable	uncontrollable	constant torque	$x_1(0)\neq 0, x_2(0)=0, x_3(0)=0$
(VI) uncontrollable	controllable	constant torque	$x_1(0)=0, x_2(0)\neq 0, x_3(0)=0$

*axis 1: maximum, 2: middle, 3: minimum

(II) $$x_1^2 = 2\mu_1\theta + A^2\sin^2\theta \quad (2\text{-}3a)$$

$$x_2 = A\cos\theta \quad (2\text{-}3b)$$

$$x_3 = A\sin\theta \quad (2\text{-}3c)$$

(III) $$x_1 = A\sinh\theta \quad (2\text{-}4a)$$

$$x_2^2 = 2\mu_2\theta - A^2\sinh^2\theta \quad (2\text{-}4b)$$

$$x_3 = A\cosh\theta \quad (2\text{-}4c)$$

where θ is the parameter determined by integrating the angular velocity along the constant control torque backward in time associated with the initial condition $\theta(0)=0$, and A is the parameter to describe the scaled angular velocity of the transient goal. Note that the manifolds for cases (IV), (V), and (VI) are omitted here, because when x_1 is swapped with x_3, the manifolds for cases (IV), (V), and (VI) are the same as those for cases (III), (I), and (II), respectively. In cases (II) and (VI), θ is not limited and the trajectories on the manifolds are open and non-periodic. In cases (III) and (IV), θ is limited and the trajectories on the manifolds are always closed and periodic. In cases (I) and (V), the trajectories on the manifolds are open or closed, depending on the parameter. Let β be a parameter defined as $\beta := |\mu_i|/A^2$ to simply obtain the separatrix between the closed and open trajectories on the manifolds for cases (I) and (V). Solving the equations $f(\beta,\theta) := 2\beta\theta - \sin^2\theta = 0$ and $f_\theta(\beta,\theta) := 2\beta - 2\sin\theta\cos\theta = 0$ with respect to β and θ yields $\beta^* \cong 0.362306$ and $\theta^* \cong 1.16556$. The scaled angular velocity of the transient goal corresponding to the separatrix, A^*, is given by $A^* = \sqrt{|\mu_i|/\beta^*}$. Note that if $\beta > \beta^*$, then θ for cases (I) and (V) is not limited, that is, the trajectories on the manifold are open and non-periodic. On the other hand, if $\beta < \beta^*$, then θ for cases (I) and (V) is limited, that is, the trajectories on the manifold are closed and periodic. The upper bounded value of parameter θ can be determined by imposing the condition that the angular velocity around the constant control torque equals zero with respect to θ for cases (III) and (IV), and under the condition $\beta < \beta^*$ for cases (I) and (V).

Figures 7(a), 7(b) and 7(c) show the manifolds for cases (I), (III) and (VI), respectively, where the scaled control torques are assumed to be unit for the sake of simplicity.

Note that the periodic parts of the manifolds are shown in Figs. 7(a) and 7(b) as open ones due to the limitation of the programming code based on Mathematica .

C. Calculation of the Points of Intersection with the Manifolds

Let α be the parameter given by $\alpha = H^2/2E$, where H is the magnitude of the angular momentum given by $H = \sqrt{(j_1\omega_1)^2 + (j_2\omega_2)^2 + (j_3\omega_3)^2}$, and E is the rotational energy of the rigid body given by $E = \left(j_1\omega_1^2 + j_2\omega_2^2 + j_3\omega_3^2\right)/2$. The intersection points between the polhode or the boosted or damped trajectory and the manifolds can be obtained numerically by using the bi-section method. There may exist several intersection points; one of these points should be selected according to control criteria, such as settling time or energy optimality. Because the control input is assumed to be constant in this paper, the point with the minimum control duration can be chosen as the energy optimal solution.

C-1. Calculation of the Intersection Point between the Polhode and the Manifolds

By replacing the constant control torque with no control torque, and introducing a new variable ψ, the polhode scaled by the variable changes given in [27] can be expressed in the form of a function of parameter ψ as follows:

For the case $\alpha \geq j_2$,

$$x_{p1} = \mathrm{sgn}(x_{p1}(0))\sqrt{x_{p1}^2(0) + \frac{D^2}{2}\left\{\cos 2\eta - \cos\left(2(\psi+\eta)\right)\right\}} \quad (2\text{-}5a)$$

$$x_{p2} = D\cos\left(\psi+\eta\right) \quad (2\text{-}5b)$$

$$x_{p3} = D\sin\left(\psi+\eta\right) \quad (2\text{-}5c)$$

where

$$D = \sqrt{x_{p2}^2(0) + x_{p3}^2(0)} \quad (2\text{-}6a)$$

$$\eta = \mathrm{a}\tan 2\left(x_{p3}(0), x_{p2}(0)\right) \quad (2\text{-}6b)$$

$$\psi(\tau) = \int_0^\tau x_{p1}(\xi)d\xi \quad (2\text{-}6c)$$

For the case $\alpha < j_2$, the expression for the polhode can be obtained by swapping x_{p1} with x_{p3} in Eqs.(2-5) and

(2-6). Note that for the case $\alpha = j_2$, the angular velocities converge to the one around the middle principal moment of inertia, and in this case, by solving $x_{p1} = x_{p3} = 0$ with respect to ψ, the range of parameter ψ is limited between 0 and $\left(\mathrm{sgn}(\eta) + \mathrm{sgn}(x_{p1}(0))\right)\pi/2 - \eta$.

An intersection point between the manifolds and the polhode can be obtained numerically by solving three equations $x_{p1} = x_1$, $x_{p2} = x_2$ and $x_{p3} = x_3$ with respect to A, θ, and ψ. Note that, as mentioned earlier, the range of phase parameter θ is limited for cases (III) and (IV), and under the condition $A > A^*$ for cases (I) and (V), and that the range of ψ is limited for the case of $\alpha = j_2$, This calculation process is repeated until all combinations of the manifolds corresponding to the constant control torque along the controllable axis are completed.

C-2. Calculation of Intersection Point between Boosted or Damped Trajectory and the Manifolds

If the scaled polhode trajectory has no intersection points with the manifolds, then, under the proposed method, the rotational motion has to be boosted or damped until it has at least one intersection point with the manifold. A typical example is the case given by a single spin motion around the uncontrollable axis. If the intersection points exist, then it is obvious that the angular velocity of an asymmetric rigid body can be stabilized to the origin by the presented piecewise steps. A problem left open is whether or not an intersection point exists between the boosted/damped trajectory and the manifolds. This problem is briefly discussed here. Note that hereafter for the purpose of simplicity, the scaled constant torque is assumed to be unit.

The rotational motion of a rigid body with damping around either the middle or minimum principal moment of inertia and boosting around the maximum principal moment of inertia is likely to converge to a flat spin motion around the maximum principal moment of inertia. The polhode near the flat spin motion is a closed loop trajectory around the axis of x_1, the manifold for case (I) is connected with the axis of x_1, and its radius around the axis of x_1 is limited within $|A^*| \cong 1.66135$, as shown in Fig. 7(a). The manifold for case (II) is also connected with the axis of x_1, but its radius around the axis of x_1 is not limited. This implies that the polhode satisfying $\alpha > j_2$ and $\sqrt{x_2^2 + x_3^2} < |A^*|$ always has an intersection point with the manifold for cases (I) and (II), and that the polhode satisfying $\alpha > j_2$ but not $\sqrt{x_2^2 + x_3^2} < |A^*|$ always intersects the manifold for case (II). Therefore, if the axis of the maximum principal moment of inertia is controllable, then to easily have an intersection point with the manifold for case (II), the following control method, which boosts around the maximum principal moment of inertia and damps around the other controllable axis, should be conducted.

$$\mu_1 = \mathrm{sgn}(x_1),\ \mu_3 = -\mathrm{sgn}(x_3) \quad \text{(angular velocity around the axis of } x_3 \text{ is controllable)} \quad (2\text{-}7a)$$

$$\mu_1 = \mathrm{sgn}(x_1),\ \mu_2 = -\mathrm{sgn}(x_2) \quad \text{(angular velocity around the axis of } x_2 \text{ is controllable)} \quad (2\text{-}7b)$$

On the other hand, if the axis around the maximum principal moment of inertia is uncontrollable, then the radius of the manifold around the axis of x_3 is not limited, and the manifold is connected with the axis of x_3, as shown in Fig. 7(c). Beside, the polhode for the case of $\alpha < j_2$ is a closed loop trajectory around the axis of x_3. This implies that polhode for the case of $\alpha < j_2$ always has an intersection point with the manifold for case (VI). Therefore, in this case, to have at least one intersection point with the manifold, the following signs should be selected for the constant control torques.

$$\mu_2 = -\mathrm{sgn}(x_2),\ \mu_3 = \mathrm{sgn}(x_3) \quad (2\text{-}8)$$

Test Problem

An example numerical simulation is conducted to demonstrate the validity of the proposed control method. It is assumed that the uncontrolled axis is around the minimum principal moment of inertia. The parameters for numerical simulation are as follows: the moments of inertia (j_1, j_2, j_3) = (15, 10, 7) [kgm^2], the constant control torque is $T_{1,2} = \pm 20$ [Nm], and the initial angular velocity vector is $(\omega_1(0),\ \omega_2(0),\ \omega_3(0)) = (1.54,\ -1.95\ -0.58)$ [rad/s]. Firstly, to determine if boosting process is needed, it is checked if the polhode intersects the manifolds. Two intersection points between the polhode and the manifold are found, and they are the angular velocity vectors (1.6296, 1.6329, -1.1622) [rad/s], and (1.6296, -1.6329, 1.1622) [rad/s], respectively. This means that no control torque is needed until reaching the manifold. The time response of the angular velocities, the time history of the control torques, the trajectory of the time and energy optimal solution along with the manifold, and the trajectory of the energy optimal but not time optimal solution are shown in Figs. 8(a), 8(b), 8(c), and 8(d), respectively. It can be seen that the angular velocities are successfully controlled to the origin by the proposed method. The time required to reach each intersection point from the initial angular velocities is determined as 1.6848[sec], and 4.1845[sec], respectively. The energy consumption of the second solution is the same as that of the first solution, but the first solution was selected from the viewpoint of the settling time in this paper. When the angular velocity vector reaches the first intersect point, the sign of the control torques is determined to be (-, 0). That is, a trajectory sliding on the manifold is generated by a negative constant control torque along the maximum principal moment of inertia.

The constant control torque is employed until the

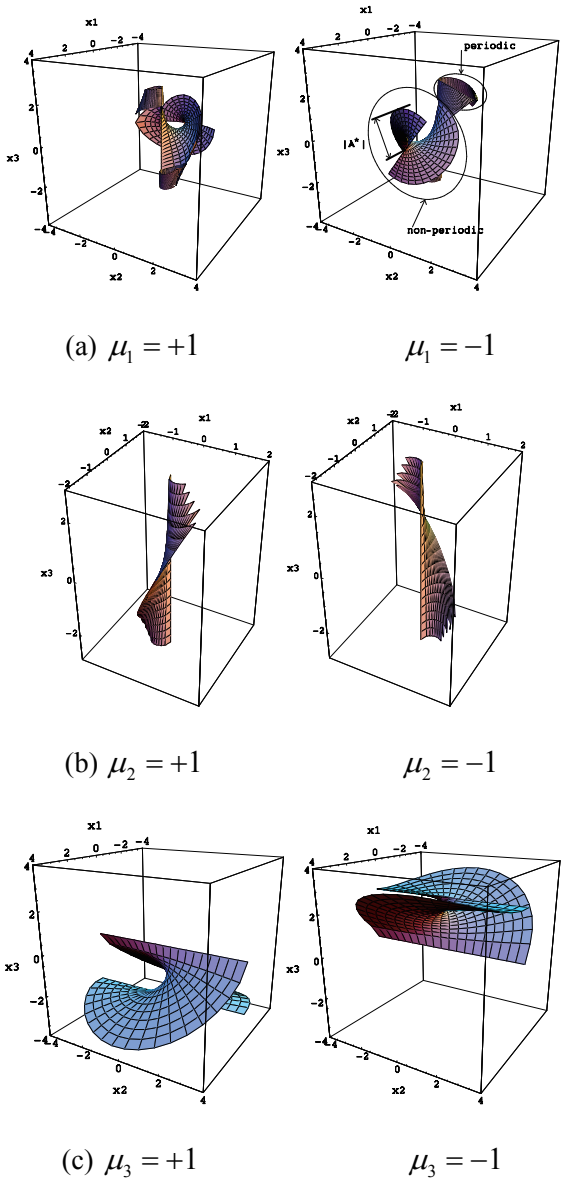

Fig. 7 Scaled constant-control manifold for case (I) (a), for case (III) (b), and for case (VI)(c).

uncontrolled angular velocity ω_3 and the one of the controlled angular velocity ω_1 converge to zero. The time required to reach the transient goal from the intersection point is found to be 1.1003[sec]. After the two angular velocities become zero, the angular velocity of the remaining controllable axis ω_2 is controlled until reaching the origin by a negative constant torque along the middle principal moment of inertia. The time required to converge to the origin from the transient goal is found to be 1.0222[sec]. The total time required to converge from the initial angular velocity to the origin is, therefore, given by

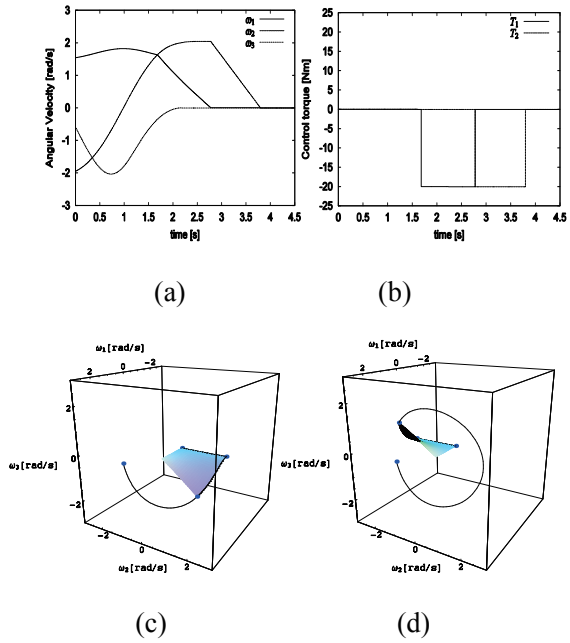

Fig.8 Time response of the angular velocities (a), time histories of the constant control torques (b), the time and energy optimal trajectory along with the intersected manifold (c), and the energy optimal but not time optimal trajectory along with the intersected manifold (d) (The start and endpoints of each segment of the trajectory are indicated by the markers).

approximately 3.8073 (1.6848 +1.1003+1.0222)[sec].

IV. Conclusion

In this paper, sliding-mode controllers have been studied for two topics related with the space debris elimination: fly-around motion control, and angular velocity stabilization by means of two-control-torque.

For the fly-around motion, a linearization feedback controller based on an exact-linearization method has been introduced in order to control the position and attitude of a chaser satellite for the purpose of constellation flight with a target satellite in the absence of a gravitational field and other disturbances. The derived controller is basically a sliding-mode controller, including the potential control inputs to avoid the singularities that take place when the line of sight is lost and the target escapes the on-board camera screen on the chaser satellite, or the attitude of the chaser satellite is opposite to that of the target satellite. In order to improve the performance of the proposed exact-linearization controller, an adaptive law has been provided for the presence of the inertia ratios uncertainty of the target. Numerical simulations have been conducted to demonstrate the effectiveness of the proposed method. The results of numerical simulations show that the proposed exact-linearization method with the adaptive law can precisely

control the position and attitude of the chaser satellite in order to track those of the target satellite by estimating the inertia ratio of the target, even if the inertia ratios uncertainty of the target satellite are included in modeling at the initial time.

For the two-control torque problem, a constant control torque method has been proposed for attenuating the rotational motion of an asymmetric rigid body. The manifold is defined as a set of the angular velocities of an asymmetrical rigid body that can approach the transient goal by employing a constant control torque, and can be obtained analytically by integrating the equations of motion backward in time from the transient goal, which is accessible from the origin by means of a single constant control torque. The obtained manifold can be used as the reference state for the sliding mode control. The trajectory resulting from the proposed method consists of three steps: First, a trajectory boosted around the maximum or minimum principal moments of inertia, and damped around the middle principal moment of inertia by control torques if necessary (if unnecessary, a trajectory of torque-free motion (polhode)) until an intersection point with the manifold is reached. Second, a trajectory sliding on the manifold, and finally a trajectory along the one controllable axis until the origin is reached. Thanks to the analytically obtained manifolds and polhode, the time required for convergence to the origin can be obtained numerically by calculating the intersection point between the manifolds and trajectories. To delete ambiguities of multiple solutions, the energy optimality and settling time is considered. The results of an example numerical simulation showed that the complete attenuation of the angular velocities of an asymmetrical rigid body can be achieved by the proposed method, provided that internal and external disturbances and modeling uncertainties are absent, and the intersection point between the trajectory and the manifold is completely obtained.

References

[1] Wie, B., Weis, H., and Arapostathis, A., "Quaternion Feedback Regulation for Spacecraft Eigenaxis Rotations", *Journal of Guidance, Control, and Dynamics*, Vol.12, No.3, 1989, pp.37-380.

[2] Bilimoria, K. D., and Wie, B., "Time-Optimal Three-Axis Reorientation of a Rigid Spacecraft", *Journal of Guidance, Control, and Dynamics*, Vol.16, No.3, 1993, pp.446-452.

[3] Steyn, W.H., "Near-Minimum-Time Eigenaxis Rotation Maneuvers Using Reaction Wheels", *Journal of Guidance, Control, and Dynamics*, Vol.18, No.5, 1995, pp.1184-1189.

[4] Hwa-Suk Oh, Young-Deuk Yoon, Young-Ken Change, Jai-Hyuk Hwang, and Sang Seok Lim, "Near-Eigenaxis Rotation Control Law Design for Moving-to-Rest Maneuver", *Journal of Guidance, Control, and Dynamics*, Vol.24, No.6, pp.1228-1231, 2001.

[5] Yuan, J.S.C., "Closed-Loop Manipulator Control Using Quaternion Feedback", *IEEE Transactions on Robotics and Automation*, Vol.4, No.4, 1988, pp.434-440.

[6] Vadali, S. R., "Variable-Structure Control of Spacecraft Large-Angle Maneuvers", *Journal of Guidance, Control and Dynamics*, Vol.9, No.2, 1986, pp.235-239.

[7] Crassidis, J. L., and Markley, F. L., "Sliding Mode Control Using Modified Rodrigues Parameters", *Journal of Guidance, Control and Dynamics*, Vol.9, No.6, 1996, pp.1381-1383.

[8] Robinett, R. D., and Parker, G. G., "Spacecraft Euler Parameter Tracking of Large-Angle Maneuvers via Sliding Mode Control", *Journal of Guidance, Control and Dynamics*, Vol.19, No.3, 1996, pp.702-703.

[9] Chen, Y. P., and Lo, S. C., "Sliding-Mode Controller Design for Spacecraft Attitude Tracking Maneuvers", *IEEE Transactions on Aerospace and Electronic Systems*, Vol.29, No.4, 1993, pp.1328-1333.

[10] Lo, S. C., and Chen, Y. P., "Smooth Sliding-Mode Control for Spacecraft Attitude Tracking Maneuvers", *Journal of Guidance, Control, and Dynamics*, Vol.18, No.6, 1995, pp.1345-1349. , 1996, pp. 1206-1211 (in Japanese).

[11] Terui, F., "Position and Attitude Control of a Spacecraft by Sliding Mode Control", *Transactions of the Japan Society of Mechanical Engineers (C)*, Vol.64, No.621, 1998, pp.215-222 (in Japanese).

[12] Isidori, A., "Nonlinear Control Systems(second edition)", Springer-Verlag, 1995.

[13] Dwyer III, T.A.W., "Exact Nonlinear Control of Spacecraft Slewing Maneuvers with Inertial Moment Transfer", *Journal of Guidance, Control and Dynamics*, Vol.9, No.2, 1986, pp. 240-247.

[14] Kida, K. and Yamaguchi, T., "On Linearization of Nonlinear Spacecraft Motion", *Transactions of the Society of Instruments and Control Engineers*, Vol.27, No.8, 1991, pp.1073-1075 (in Japanese).

[15] Yamada, K., Yoshikawa, S., Yoshida, N., and Koyama, H., "Relative Motion Control Between Spacecraft", *Transactions of the Society of Instruments and Control Engineers*, Vol.30, No.10, 1994, pp. 1225-1233 (in Japanese).

[16] Crouch, P.E., "Spacecraft Attitude Control and Stablilization: Application of Geometric Control Theory to Rigid Body Model," IEEE Transactions on Automatic Control, Vol.29, No.4, 1984, pp.321-331.

[17] Brockett, R.W., "Asymptotic Stability and Feedback Stabilization," Differential Geometric Control Theory, Birkhauser, Boston, 1983, pp.181-208.

[18] Aeyels, D., "Stabilization by Smooth Feedback Control of the Angular Velocity of a Rigid Body," Systems and Control Letters, Vol.6, No. 1, 1985, pp.59-63.

[19] Aeyels, D., and Szafransski, M., "Comments on the Stabilizability of the Angular Velocity of a Rigid Body", Systems and Control Letters, Vol.10, No.1, 1988, pp.35-39.

[20] Sontag, E.D., and Sussman, H.J., "Futher Comments on the Stabilizability of the Angular Velocity of a Rigid Body," Systems and Control Letters, Vol.12, No. 3, 1988, pp.213-217.

[21] Outbib, R. and Sallet, G., "Stabilizability of the Angular Velocity of a Rigid Body Revisited," Systems & Control Letters, Vol. 18, No. 2, 1992, pp.93-98.

[22] Andriano, A., "Global Feedback Stabilization of the Angular Velocity of a Symmetric Rigid Body," Systems and Control Letters, Vol. 20, No.5, 1993, pp.361-364.

[23] Tsiotras, P., and Schleicher, A. "Detumbling and Partial Attitude Stabilization of a Rigid Spacecraft under Actuator Failure," AIAA Paper 00-4044, 2000.

[24] Astolfi, A. and Rapaport, A., "Robust Stabilization of the Angular Velocity of a Rigid Body," Systems & Control Letters, Vol.34, No. 5, 1998, pp.257-264.

[25] Astolfi, A., "Output Feedback Stabilization of the Angular Velocity of a Rigid Body," Systems & Control Letters, Vol. 36, No.3, 1999, pp.181-192.

[26] Mazenc, F. and Astolfi, A., "Robust Output Feedback Stabilization of the Angular Velocity of a Rigid Body," Systems & Control Letters, Vol. 39, No. 3, 2000, pp.203-210.

[27] Livnch, R., and Wie, B., "New Results for an Asymmetric Rigid Body with Constant Body-Fixed Torques," AIAA Journal of Guidance, Control, and Dynamics, Vol.20, No.5, 1997, pp.873-881.